International Journal of Non-Linear Mechanics 70 (2015) 20–29

Contents lists available at ScienceDirect

International Journal of Non-Linear Mechanics

journal homepage: www.elsevier.com/locate/nlm

The application of inerter in tuned mass absorber

P. Brzeski [a], E. Pavlovskaia [b], T. Kapitaniak [a], P. Perlikowski [a,*]

[a] Division of Dynamics, Technical University of Lodz, Stefanowskiego 1/15, 90-924 Lodz, Poland
[b] Centre for Applied Dynamics Research, School of Engineering, University of Aberdeen, AB24 3UE, Aberdeen, Scotland

ARTICLE INFO

Article history:
Received 11 March 2014
Accepted 8 October 2014
Available online 19 October 2014

Keywords:
Inerter
Duffing oscillator
Tuned mass absorber
Pendulum
Bifurcation analysis
Optimization

ABSTRACT

In this paper we investigate the dynamics of tuned mass absorber with additional viscous damper and inerter attached to the pendulum. The devices are used to damp out oscillations of non-linear Duffing oscillator. Analysis of how these devices influence the dynamics of tuned mass absorber and its damping properties is shown. We calculate the detailed bifurcation diagrams and show how by changing the parameters of damper and inerter one can eliminate dangerous dynamic instabilities from the systems. Finally, in the last section we present an optimization of TMA's parameters in order to achieve best efficiency in damping of the main body vibrations.

1. Introduction

The effective damping of mechanical and structural systems oscillations has always been a big challenge for engineers. One of the first attempts to absorb energy of vibrations and in consequence reduce the amplitude of motion is a tuned mass damper (TMD) introduced by Frahm [1]. The device consists of mass on linear spring such that its natural frequency is identical with the natural frequency of damped system. As it is well known, classic TMD is extremely effective in reducing response of the main structure in its resonance but for other frequencies (even close to this resonant frequency) it increases the amplitude of the system's motion.

Modification of TMD has been presented in the work of Den Hartog [2]. The author proposes the addition of the viscous damper to Frahm's system design. Thanks to introduced damping TMD become a powerful device that can reduce vibrations of the main body in a wide range of excitation frequencies around principal resonance. Another modification that can lead to broaden the range of TMD effectiveness has been proposed by Roberstson [3] and Arnold [4], who interchange linear spring of the TMD by the non-linear one (with linear and non-linear parts of stiffness). In recent years much more attention has been paid to the possibility of using purely non-linear springs [5–7]. Authors show that systems with such springs have no main resonant frequency, hence the TMD works in a wide range of excitation frequencies.

One can find many successful applications of TMDs which are used to prevent damage of buildings due to seismic excitation [8,9], suppress vibration of tall buildings subjected to wind [10,11], achieve the best properties of cutting processes [12,13], decrease vibration of floors or balconies [14,15], reach stable rotations of rotors [16–18], stabilize drilling strings [19] and many others.

Another important contribution into subject of vibrations absorption is an introduction of the device called a tuned mass absorber (TMA) proposed by Hatwal et al. [20–22] who interchange the linear/non-linear oscillator by the pendulum. In case of pendulum the natural frequency depends only on its length, so TMA it much easier to tune in practical applications. Moreover, the disadvantage of TMD is that it works only along its mounting direction. This drawback is not present for the TMA because pendulum can oscillate regardless of the direction of base structure motion (in horizontal case pendulum oscillates for any excitation frequency while for vertical orientation only in its parametric resonances). The dynamics of the TMA with vertical forcing of base oscillator is considered in a few papers [21–31]. Presented analysis allows to understand the dynamics and response of the main structures around primary and secondary resonances of the pendulum. The complete bifurcation analysis of the TMA applied to vertically forced Duffing oscillator in two parameters space (amplitude and frequency of excitation) is presented in [32]. The similar analysis is also performed for systems with horizontally forced main masses [33–36].

In our previous paper [37] we show the detailed analysis of TMA with additional damper in the pivot of pendulum. We show that properly chosen value of pendulum's damping coefficient can strongly decrease the amplitude of Duffing oscillator around primary resonance and broaden the range of TMA effectiveness.

* Corresponding author.
E-mail address: przemyslaw.perlikowski@p.lodz.pl (P. Perlikowski).

http://dx.doi.org/10.1016/j.ijnonlinmec.2014.10.013
0020-7462/

We also present optimization scheme that can be used to determine optimum values of damping parameters. In this paper we develop this idea and consider system with not only additional damper but also the inerter. The inerter is a two terminal element which has the property that force generated at its ends is proportional to the relative acceleration between them [38]. Smith proposed to use an inerter in suspensions of cars. He has shown that oscillations induced by road imperfections and load disturbances can be reduced more effectively using suspensions with inerters. In his further work [39] he has studied several simple passive suspension struts, each containing at most one damper and inerter. The theoretical results are confirmed by experiment showing that suspension layouts with inerter are more effective than classical designs with damper and springs only. In 2005 the inerter has been profitably used as a part of suspension in Formula 1 racing car [40]. Wang and Su [41] present how the performance of suspension is influenced by non-linearities which appear due to the inerter construction including effects caused by friction, backlash and elasticity. They show that the performance benefits are slightly degraded by the inerter non-linearities but still the overall performance of suspension with a non-linear inerter is better than traditional suspensions, especially when the stiffness of suspension is large. As one can expect successful application of an inerter in car suspension resulted in a number of studies on other possible applications of inerters. Takewaki et al. examine [42] if the advantages of inerter can be beneficial in devices protecting buildings from earthquakes. The authors present detailed study showing how allocation of damping device with inerter on each storey (from first to twelve storey) influences the response of the building. In a recent paper [43] authors study the influence of inerter on the natural frequencies of vibration systems. They propose different constructional solutions of one and two degree-of-freedom systems and present how inerters influence their dynamics.

This paper is organized as follows: Section 2 contains description of the considered model of the system. Section 3 is divided into three parts. In the first part we show the influence of additional viscous damper on performance of TMA, the second part is devoted to influence of inerter and in the last one we compare how these devices affect the dynamics of the system. Finally, in Section 4, we consider the dynamics of the system under the presence of both damper and inerter and use optimization procedure to obtain the optimal values of additional devices parameters which ensure the best damping properties. We summarize our results in Section 5.

2. Model of the system

We consider a horizontally forced single-well Duffing oscillator with attached T-shaped pendulum (Fig. 1(a)). Additional devices – damper and inerter are mounted onto the base structure and attached to the ends of the arms of the T-shaped pendulum. The motion of the system is characterized by following generalized coordinates: the horizontal displacement of Duffing oscillator is described by coordinate x and the angular displacement of pendulum is given by angle φ. The notation of systems' parameters is as follows: M is mass of Duffing oscillator, m and l correspond to mass and length of pendulum's rod, l_a is the length of the massless cross arms of T-shaped pendulum, k_1 and k_2 are linear and non-linear parts of spring stiffness. The viscous damping coefficient of Duffing oscillator is given by c and the viscous damping in the pivot point of the pendulum by c_P. Inertance of the inerter connected to the pendulum is given by parameter I_n while c_A is damping coefficient of additional viscous damper.

In Fig. 1(b) we present considered system with deflected pendulum. In order to derive the equations of motion we have to calculate the generated forces in the additional devices with the change of angular position of the pendulum φ. The change in the length of additional damper Δl_{damper} can be calculated as follows:

$$\Delta l_{damper} = -\frac{l_a \sin\varphi}{\cos\alpha_d}, \tag{1}$$

where l_a is the length of the pendulum's arm and α_d is an angle by which the damper is deflected from the vertical position. To calculate the change in the length of inerter $\Delta l_{inerter}$ the following formula can be used

$$\Delta l_{inerter} = \frac{l_a \sin\varphi}{\cos\alpha_i}, \tag{2}$$

where α_i is an angle by which the inerter is deflected from the vertical position. As discussed in Appendix A the system can be designed to ensure that $\alpha_d \ll 1$ and $\alpha_i \ll 1$ which enables us to simplify Eqs. (1) and (2):

$$\Delta l_{damper} = -l_a \sin\varphi, \tag{3}$$

$$\Delta l_{inerter} = l_a \sin\varphi, \tag{4}$$

hence:

$$\Delta \dot{l}_{damper} = -l_a\dot{\varphi}\cos\varphi \quad \Delta \ddot{l}_{damper} = -l_a\ddot{\varphi}\cos\varphi + l_a\dot{\varphi}^2\sin\varphi, \tag{5}$$

$$\Delta \dot{l}_{inerter} = l_a\dot{\varphi}\cos\varphi \quad \Delta \ddot{l}_{inerter} = l_a\ddot{\varphi}\cos\varphi - l_a\dot{\varphi}^2\sin\varphi. \tag{6}$$

Using the above calculated velocities we can derive the following formula for the kinetic energy T, potential energy V, Rayleigh dissipation D and general forces Q for the considered system:

$$T = \frac{1}{2}(M+m)\dot{x}^2 + \frac{1}{6}ml^2\dot{\varphi}^2 + \frac{1}{2}ml\dot{x}\dot{\varphi}\cos\varphi + \frac{1}{2}I_n(\Delta\dot{l}_{inerter})^2 \tag{7}$$

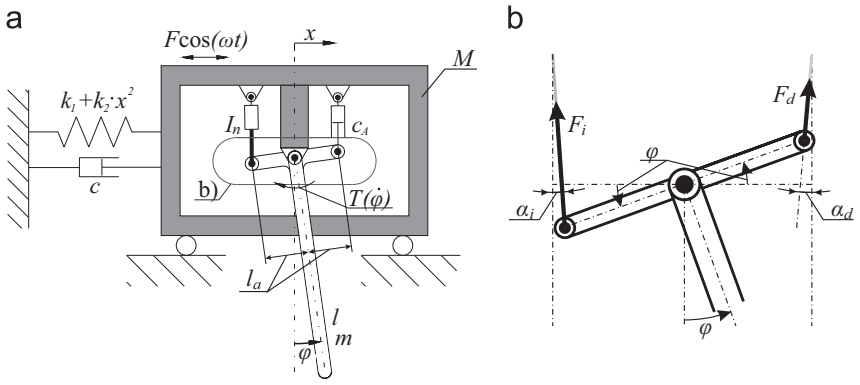

Fig. 1. Model of the system (a) and orientation of forces generated by additional devices (b).

$$V=\frac{1}{2}k_1x^2+\frac{1}{4}k_2x^4-\frac{1}{2}mlg\cos\varphi \tag{8}$$

$$D=\frac{1}{2}c\dot{x}^2+\frac{1}{2}c_A(\Delta\dot{l}_{damper})^2 \tag{9}$$

$$Q=T(\dot{\varphi})\frac{\partial\varphi}{\partial\varphi} \tag{10}$$

where $T(\dot{\varphi})=c_P\dot{\varphi}$ is a damping momentum in the pivot point of the pendulum. Using Lagrange equations off the second type we get the equations of motion:

$$(M+m)\ddot{x}+\frac{1}{2}ml\left[\ddot{\varphi}\cos\varphi-\dot{\varphi}^2\sin\varphi\right]+k_1x+k_2x^3+c\dot{x}=F\cos(\omega t) \tag{11}$$

$$\frac{1}{2}ml\ddot{x}\cos\varphi+\left(\frac{1}{3}ml^2+I_nl_a^2\cos^2\varphi\right)\ddot{\varphi}+\frac{1}{2}mlg\sin\varphi +(c_P+c_Al_a^2\cos^2\varphi)\dot{\varphi}-I_nl_a^2\dot{\varphi}^2\cos\varphi\sin\varphi=0 \tag{12}$$

Introducing dimensionless time $\tau=t\omega_1$, where $\omega_1=\sqrt{k_1/M}$ is the linear approximation of natural frequency of Duffing oscillator we obtain dimensionless equations:

$$(1+m_D)\tilde{x}''+\frac{1}{2}m_Dl_D\left[\varphi''\cos\varphi-(\varphi')^2\sin\varphi\right]+\tilde{x}+k_{2D}\tilde{x}^3+c_D\tilde{x}'=F_D\cos(\tilde{\omega}\tau) \tag{13}$$

$$\frac{1}{2}m_Dl_D\tilde{x}''\cos\varphi+\left(\frac{1}{3}m_Dl_D^2+I_{nD}l_{aD}^2\cos^2\varphi\right)\varphi''+\frac{1}{2}m_Dl_Dg_D\sin\varphi +(c_{PD}+c_{AD}l_{aD}^2\cos^2\varphi)\varphi'-I_{nD}l_{aD}^2(\varphi')^2\cos\varphi\sin\varphi=0 \tag{14}$$

where prime denotes the differentiation with respect to non-dimensional time τ, $\tilde{x}=x/l_0$, $\tilde{x}'=\dot{x}/l_0\omega_1$, $\tilde{x}''=\ddot{x}/l_0\omega_1^2$, $\varphi'=\dot{\varphi}/\omega_1$, $\varphi''=\ddot{\varphi}/\omega_1^2$, (for simplicity tildes in dimensionless equations will henceforth be omitted) $k_{2D}=k_2l_0^2/M\omega_1^2$, $c_D=c/M\omega_1$, $c_{PD}=c_P/Ml_0^2\omega_1$, $c_{AD}=c_A/M\omega_1$, $I_{nD}=I_n/M$, $l_D=l/l_0$, $l_{aD}=l_a/l_0$, $m_D=m/M$, $g_D=g/l_0\omega_1^2$, $F_D=F/Ml_0\omega_1^2$, $\tilde{\omega}=\omega/\omega_1$.

We take initial parameters values from our previous paper [37] which are as follows: $M=3.63$ [kg], $k_1=660$ [N/m], $k_2=200$ [N/m], $c=0.240$ [Ns/m], $c_P=1.977$ [Nms], $l=0.0779$ [m], $l_a=0.01$ [m], $m=0.363$ [kg], $F=0.33$ [N]. Values of parameters c_{AD} and I_{nD} which are used to describe the additional damper and inerter respectively will be changed during numerical simulations in order to show how these supplementary devices influence the efficiency of the TMA and the dynamics of the considered system.

Using reference length $l_0=1.0$ [m] we perform transformation to dimensionless parameters (depicted by letter D) in a way that allows to hold accessibility to physical parameters receiving: $k_{2D}=0.30303$, $c_D=0.0049$, $c_{PD}=4.04\times10^{-2}$, $l_D=0.0779$, $l_{aD}=0.01$, $m_D=0.1$, $g_D=0.053955$, $F_D=0.0005$.

3. Numerical results

3.1. Influence of additional damper on the response of the Duffing oscillator

In our previous paper [37] we have investigated the dynamics of the horizontally forced Duffing oscillator with suspended TMAs of three different types, i.e., classical single pendulum, dual pendulum and pendulum-spring. We have shown how different parameters of TMAs affect the behavior of the system and then proposed an optimization method which can be used to adjust the absorbers parameters to obtain the best damping properties in a wide range of excitation frequencies. One of the main conclusions drawn from the analysis of single pendulum TMA is that damping coefficient in the pivot point of the pendulum has a decisive influence on the device efficiency. When damping coefficient is too small one can observe the decrease of Duffing oscillator amplitude only around principal resonance and when it is too big, TMA barely changes the response of the base structure. In real world applications it can be difficult to ensure specifically identified value of viscous damping coefficient in the pivot point of the pendulum. Therefore, in this paper we propose the modification of the pendulum's design (by introducing T-shaped pendulum) that allows the attachment of oil viscous damper or a magnetorheological damper. Thus, total damping of the pendulum consists of two components: damping in the pivot point described by parameter $c_{PD}=4.04\times10^{-2}$ which is equivalent to 1% of critical damping of the pendulum and damping introduced by additional damper described by parameter c_{AD}. In this case the total damping of the pendulum can be easily controlled. To show dynamics of Duffing system under the presence of additional damper in detail we present how frequency response curve (FRC) changes for increasing value of c_{AD}. To obtain the FRC we use the Auto 07p [44] continuation toolbox. In Fig. 2(a) we present FRCs calculated for the system without additional damper (in this case we consider only damping in the pivot point) and for the system with additional viscous damper characterized by parameter $c_{PD}=5.5\times10^{-2}$. In both cases we assume that there is no inerter attached to the arm of the pendulum ($I_{nD}=0$).

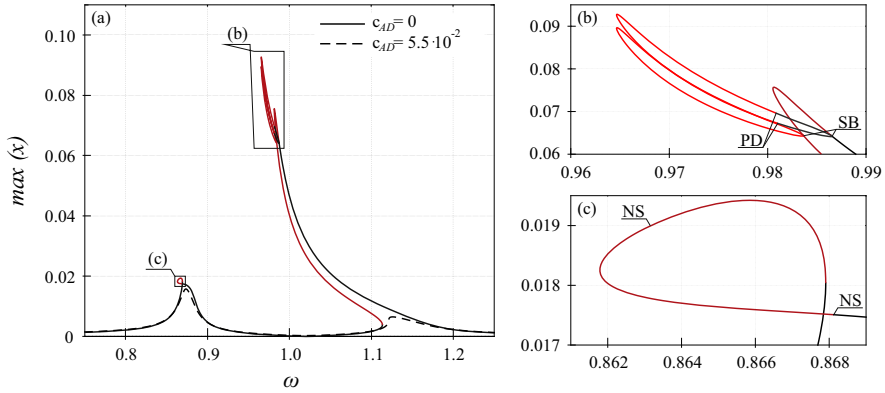

Fig. 2. FRCs of the base structure calculated for the system without inerter ($I_{nD}=0$): with no additional damper $c_{AD}=0$, (continuous line) and with additional damper $c_{AD}=5.5\times10^{-2}$ (dashed line) showing how the increase of pendulum's total damping coefficient influences the response of the base structure. Subplots (b,c) are magnifications of FRC curve presented in subplot (a). The stability of solutions is depicted by color of lines: black color corresponds to stable and red color to unstable solutions. The damping in pivot of pendulum is present for both cases. (For interpretation of the references to color in this figure caption, the reader is referred to the web version of this paper.)

Along the solid line presented in Fig. 2(a) that corresponds to the system without additional damper one can see the following bifurcations: for $\omega = 0.867907$, $\omega = 0.861789$, $\omega = 1.11276$, $\omega = 0.980540$ saddle-node bifurcations occur, for $\omega = 0.863156$, $\omega = 0.868125$ Neimark–Sacker bifurcations appear and for $\omega = 0.983657$, $\omega = 0.9865495$ symmetry breaking pitchfork bifurcations occur. The two asymmetric solutions created in pitchfork bifurcation lose their stability in a period doubling bifurcations that occur for $\omega = 0.980868$, $\omega = 0.981021$. Bifurcations described above give rise to the coexistence of different attractors which can be observed in a wide range of excitation frequency ω. Therefore, the dynamics of the considered system without additional damper is complicated and such a design is inconvenient for practical applications. Dashed line presented in Fig. 2(a) is calculated for the system with additional damper characterized by parameter $c_{AD} = 5.5 \times 10^{-2}$. Due to the presence of supplementary damper, total damping coefficient of the pendulum rises causing the decrease of Duffing amplitude and elimination of all bifurcations. To present how the position of each bifurcation on the FRC changes with increase of the damping coefficient of additional damper, we calculated two parameters bifurcation diagram (ω, c_{AD}) presented in Fig. 3. Analyzing bifurcation curves presented in Fig. 3 one can see that Neimark–Sacker bifurcations disappear if $c_{AD} > 0.656 \times 10^{-2}$ (which corresponds to about 0.16% of critical damping), and symmetry breaking bifurcations vanish for $c_{AD} > 1.214 \times 10^{-2}$ (0.3% of critical damping). Therefore if damping coefficient of additional damper is greater than 0.3% of critical damping one will observe only symmetric periodic solutions of the system. To eliminate all bifurcations and receive FRC without any coexistence of attractors one has to ensure that $c_{AD} > 5.196 \times 10^{-2}$ meaning that additional damper damping coefficient is greater than 1.29% of critical damping. All above values are relatively small. Moreover, as we proved in our previous publication [37] for system with given parameters best damping efficiency of TMA can be achieved if total damping coefficient of the pendulum is equal to about 18% of critical damping. Therefore if additional damper damping coefficient is close to the optimal value it will be effective with both suppressing the system's response as well as elimination of dangerous dynamical phenomena. We do not show period doubling bifurcations of asymmetric solutions because they disappear simultaneously with pitchfork bifurcations.

3.2. Influence of the inerter on the response of the Duffing oscillator

As we mentioned before, there are no previous studies on application of inerter in TMA. Hence, the influence of the inerter on damping properties of TMAs needs to be carefully examined. Similar to previous paragraph, to show how the dynamics of Duffing system changes under the presence of inerter, FRCs are used. Such approach enables accurate description of how the value of additional inertance attached to the T-shaped pendulum (I_{nD}) affects dynamical response of the system and damping properties of TMA. In Fig. 4 (a) we show two FRCs, solid line corresponds to the system without the inerter, and dashed one to system with additional inerter described by dimensionless parameter $I_{nD} = 22.5$. In both cases we assume that there is no additional damper ($c_{AD} = 0$) therefore damping is present only in the pivot of the pendulum and it is equal to 1% of critical damping ($c_{PD} = 4.04 \times 10^{-2}$). Black line presented in Fig. 4(a) is identical to the one presented in Fig. 2(a) and should be used as a reference. Analysis of dashed FRC presented in Fig. 4 (a) proves that by addition of the inerter one can eliminate all bifurcations that occur along the FRC of base structure. Simultaneously, we see that the influences of inerter and additional damper on the systems dynamics is different.

Two parameters bifurcation diagram (ω, I_{nD}) shown on Fig. 5 details the influence of the additional inertance on position of each bifurcation along the FRC. For the system without inerter – regardless of total pendulum damping coefficient – all bifurcations occur in the range $\omega \in (0.85, 1.15)$. Addition of inerter causes the shift in the bifurcations position towards the smaller values of forcing frequency. Therefore, the range of parameter ω for which we can observe saddle-node bifurcations rapidly moves towards smaller values of ω. Analyzing bifurcation curves shown in Fig. 5 one can see that Neimark–Sacker bifurcations disappear if $I_{nD} > 0.143$, and symmetry breaking bifurcations vanish for $I_{nD} > 1.436$. This means that even for the system without additional damper we can eliminate non-periodic and non-symmetric solutions by the introduction of the inerter. Unfortunately, the elimination of all bifurcations requires relatively high inertance values, and it can be achieved for $I_{nD} > 20$ which means that inerter has 20 times bigger inertia than the Duffing oscillator. Such device can be easily constructed by the use of multi-stage gear unit but it would completely mitigate pendulum's motion and eliminate the damping properties of TMA (see FRC calculated for $I_{nD} = 22.5$ presented in Fig. 4(a)). However, it is important to notice that the range of coexistence of different solutions caused by saddle-node bifurcations is extremely small if $I_{nD} > 4$.

3.3. Comparison of the inerter and the damper influences

In Sections 3.1 and 3.2 we presented how the damper and the inerter influence the dynamical response of the Duffing oscillator.

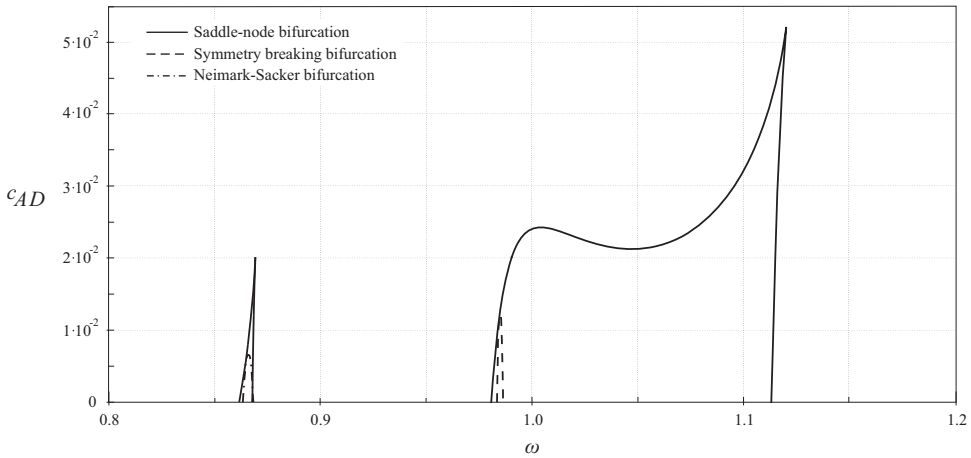

Fig. 3. Two parameters bifurcation diagram (ω and c_{AD}) showing how the value of additional damper damping coefficient affects the position of bifurcation points on the FRCs. The damping in pivot of pendulum is present.

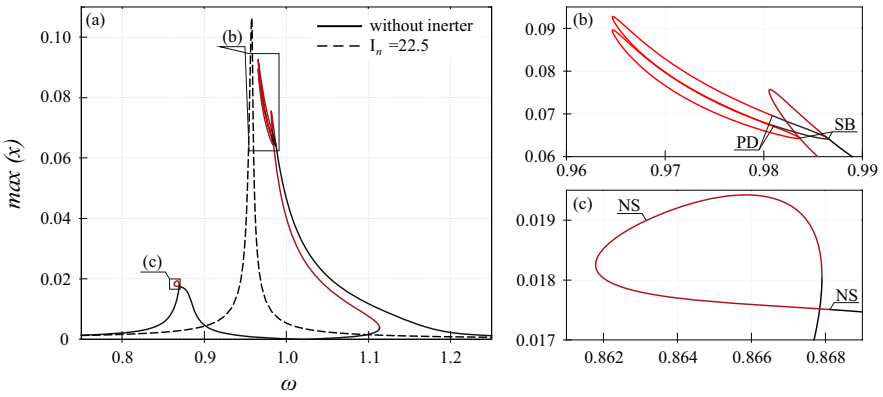

Fig. 4. FRCs of the base structure calculated for system without inerter and additional damper ($c_{AD}=0$, $I_{nD}=0$) (solid line) and for the system with inerter only $I_{nD}=22.5$ (dashed line) showing how the addition of inerter influences the response of the base structure. Subplots (b,c) are magnifications of FRC curve presented in subplot (a). The stability of solutions is depicted by color of lines: black color corresponds to stable and red color to unstable solutions. The damping in pivot of pendulum is present for both cases. (For interpretation of the references to color in this figure caption, the reader is referred to the web version of this paper.)

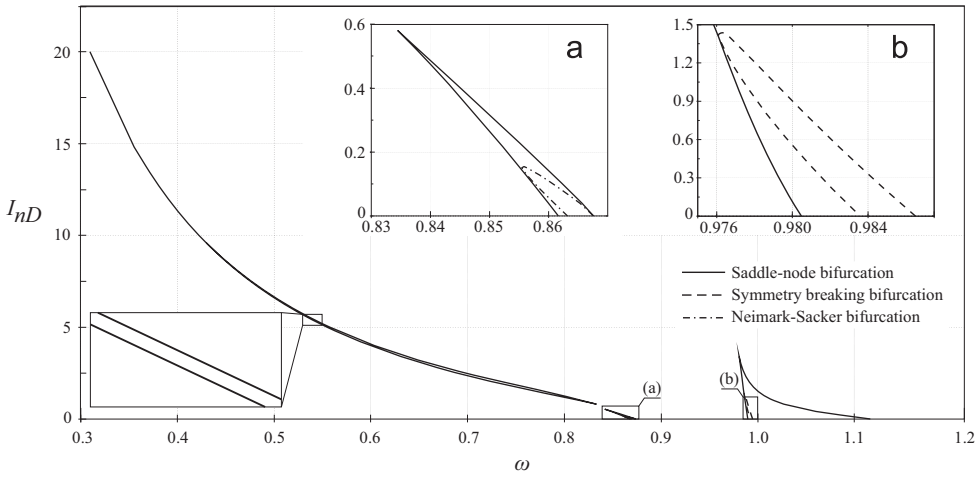

Fig. 5. Two parameters bifurcation diagram (ω and I_{nD}) showing how the value of additional inertance affects the position of bifurcation points on the FRCs. The damping in pivot of pendulum is present.

In this section we compare the effects caused by these devices. Results presented in Figs. 3 and 5 can be used to correlate how additional damper and inerter change the response of base structure by shifting the position of the bifurcations. In both Figs. 3 and 5 bottom horizontal line of the graph refers to lack of these devices ($c_{AD}=0$, $I_{nD}=0$). The FRC for such case is presented both in Figs. 2(a) and 4(a) and is used as a reference line. When we introduce the additional damper to the system, we see that even if its damping coefficient is relatively small it is easy to eliminate all bifurcations. If we want to use only an inerter to eliminate all bifurcations it should have comparatively high inertance value. Despite the value of parameter c_{AD} all bifurcations occur in range $\omega \in (0.85,\ 1.15)$ but the increase of inertance parameter I_{nD} leads to extension of this range towards smaller values of forcing frequency ($\omega \in (0.31,\ 1.12)$). When the damping coefficient rises we initially observe rejection of bifurcations that occur around first resonance peak ($\omega \approx 0.87$). If $c_{AD} > 2\times 10^{-2}$ we observe only saddle-node bifurcations (two or four) around second resonance peak ($\omega \approx 0.87$). Contrary, with increase of additional inertance we firstly observe elimination of bifurcations that occur around second resonance peak. Two saddle-node bifurcations endure up to $I_{nD}=20$ but distance between them is extremely small and with the increase of I_{nD} their position shifts towards smaller values of ω (up to $\omega=0.3$).

To further analyze the difference between the effects that are caused by inerter and damper we calculated six FRCs of considered system that are presented in Fig. 6. Three of them correspond to the system with different inerters attached only, and other three shows the response of the system in a presence of different additional dampers only. In the upper row we show the response of Duffing oscillator, while in the lower row the maximum amplitude of pendulum versus frequency of excitation ω.

First two subplots of Fig. 6 presents the changes in the dynamic response of Duffing oscillator. Analyzing Fig. 6(a) one can say that increase of additional inertance leads to the following effects: first resonance peak becomes much smaller while second one is slowly rising. Both peaks occur for the smaller ω as I_{nD} increases. If we substitute inerter with damper (see Fig. 6(b)) and increase damping coefficient we notice that two resonance peaks merge into one that arise around $\omega=0.95$. But the most essential effect of total damping coefficient increase is the significant reduction of the peak height which cannot be observed in system with inerter only. Hence, while inerters can be used for elimination of bifurcations, they do not affect damping properties positively. Subplots (c,d) in Fig. 6 refer to the response of the pendulum. Analysis of Fig. 6 (d) leads to conclusion that by addition of damper which is attached to the arm of T-shaped pendulum we can easily decrease its motion amplitude in a wide range of forcing frequencies. Moreover, this effect is present even for relatively small damping coefficients (see dashed curve presented in Fig. 6(d) calculated for $c_{AD}=0.404$ which corresponds to 10% of critical damping). If we want to suppress pendulum's motion with comparable effectiveness we have to use

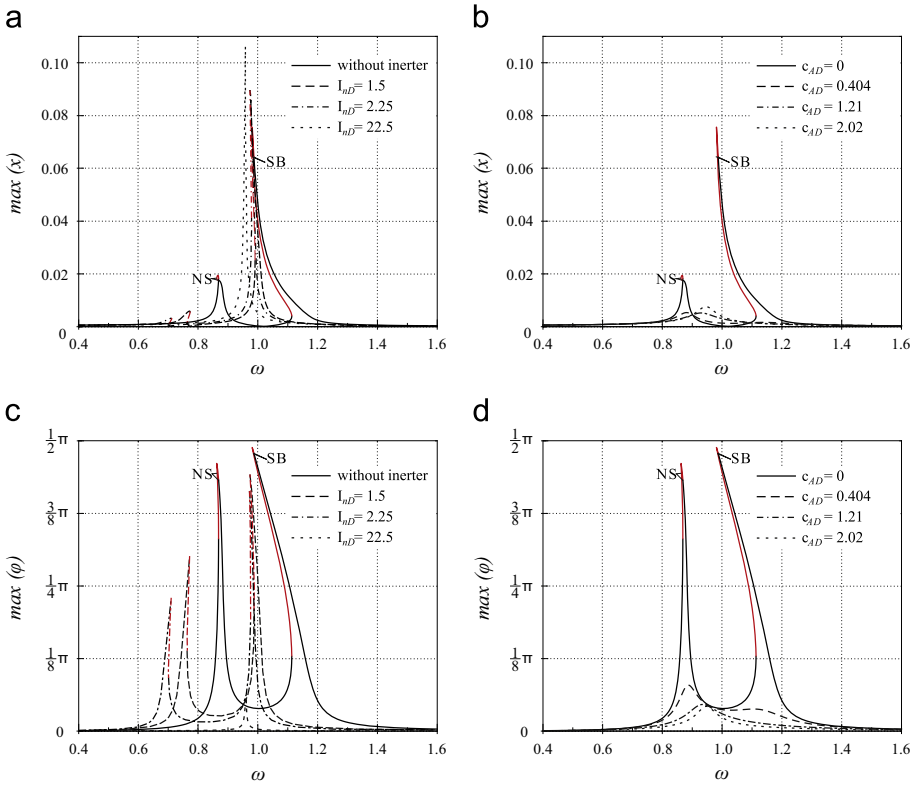

Fig. 6. Comparison between systems with attached inerter and additional damper. (a,b) FRCs of Duffing oscillator and (c,d) FRCs of pendulum calculated for systems with three different inerters (a,c), and three different dampers (b,d). For plots in each column parameters of the systems are identical.

inerter with comparatively high inertance (see dotted line presented in Fig. 6(c) calculated for $I_{nD}=22.5$). Otherwise, with the increase of parameter I_{nD} we observe slow reduction in peaks height and their migration toward smaller forcing frequencies.

4. Optimization of additional devices parameters

Up to this moment we considered systems with only one additional device (damper or inerter). Such approach allow us to compare the effects caused by both devices and to emphasize differences between their influence on systems dynamics. We claim that a combination of both inerter and additional damper can lead to boost in TMA's damping efficiency. In this section we validate this assumption and present how the response of base structure changes for different values of parameters I_{nD} and c_{AD}.

In order to visualize the behavior of the system with both inerter and additional damper in Fig. 7(a,b,e,f) we present three dimensional plots created as a surfaces based on the FRCs of the system. To give better overview of the Duffing system amplitude we also present two dimensional maps which are flat projections of three dimensional surfaces presented in subplots (c,d,g,h) of Fig. 7. For each plot we assume different additional damper coefficient and present how inertance value influences response of Duffing oscillator changing I_{nD} from 0 to 1. In this section we confine considered range of I_{nD} because TMA damping efficiency deteriorate for higher values of I_{nD}. Plots (a,c) were calculated for $c_{AD}=0.202$ which equals to 5% of critical damping, plots (b,d) for $c_{AD}=0.404$ which stands for 10% of pendulum critical damping, subplots (e,g) represent the response of the system for $c_{AD}=0.808$ (20% of critical damping) and (f,h) for $c_{AD}=1.212$ (30% of critical damping). Analyzing Fig. 7 one can say that for every considered value of damping coefficient one can achieve the decrease of Duffing oscillator amplitude by addition of proper inerter. This effect is highly visible for smaller values of c_{AD} when the addition of inerter helps to improve TMA's efficiency significantly for a wide range of ω.

Analyzing the results obtained for $c_{AD}=0.202$ (Fig. 7(a,c)) we see that for system without inerter first resonance peak which occurs around $\omega=0.85$ is dominant. If we introduce inerter and increase parameter I_{nD} we see that the height of first resonance peak decreases while second resonance peak is growing and becomes dominant for $I_{nD}>0.5$. Similar phenomena can be observed for the system with increased additional damping coefficient $c_{AD}=0.404$ (Fig. 7(a,c)). The only difference is that because total damping coefficient of the pendulum is closer to optimal value both resonance peaks are smaller and less slender. If we increase additional damper damping coefficient up to 20% of critical damping ($c_{AD}=0.808$) we observe only one resonance peak (Fig. 7(e,g)). For the system without inerter, it occurs around $\omega=0.9$. If we introduce inerter and increase supplementary inertance I_{nD}, we also observe migration of the peak's position towards higher values of excitation frequencies. Decrease in the amplitude of base structure can be observed for $I_{nD}\approx 0.5$ but it is not so significant as for smaller values of c_{AD}. Effects caused by an inerter are similar to $c_{AD}=1.212$ (Fig. 7(f,h)) but for this case improvement in damping efficiency is barely visible. Therefore, if total damping coefficient of the pendulum is relatively large (in our case greater than 30% of critical damping) it suppress pendulum's vibrations so much that inerter's influence on its dynamics is barely visible.

Comparing results obtained for damping coefficients equal to 10% and 20% of critical damping, we see that comparable damping efficiency can be achieved for different composition of parameters c_{AD} and I_{nD}. Still, by changing the configuration of different dampers and inerters, we can better adjust the shape of FRC to our expectations. Moreover, in many cases inerters can be easier and more convenient to apply precise inertance value.

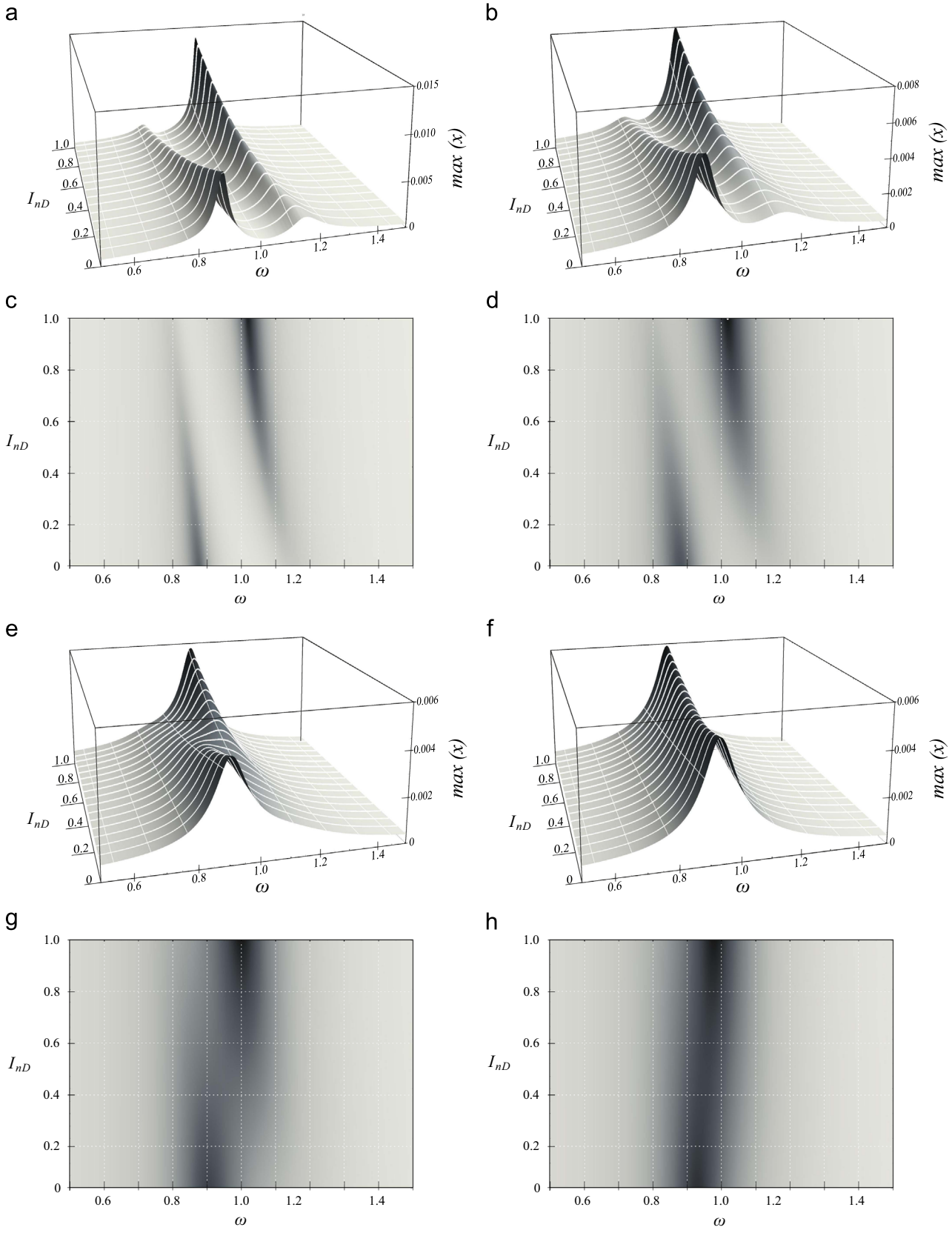

Fig. 7. Three dimensional plots presenting FRC of the system with inerter and additional damper (a, b, e, f) and two dimensional maps (c, d, g, h) which are flat presentations of subplots (a, b, e, f) respectively. Plots (a, c) were calculated for $c_{AD} = 0.202$ (5% of critical damping), plots (b, d) for $c_{AD} = 0.404$ (10% of critical damping) and plots (e, g) for $c_{AD} = 0.808$ (20% of critical damping) and (f, h) for $c_{AD} = 1.212$ (30% of critical damping).

5. Conclusions

In this paper we examine how additional devices attached to the T-shaped pendulum TMA influences the dynamical response of base structure. In the beginning we propose change in the pendulum's shape and analyze its consequences. Introduction of the T-shaped pendulum enables easier control of total damping coefficient of the pendulum and allows the addition of other supplementary devices that can modify the response of the system. Simultaneously, changes in the TMA design can be conducted in a way that would not cause undue complexity of the model. Therefore, we claim that proper modification of pendulum's shape can significantly facilitate process of adjusting TMA performance to required level.

In Section 3 we investigated how additional damping and inertance introduced by supplementary devices influence the system dynamics and compare the effects caused by additional damper and inerter. Addition of both components can lead to elimination of bifurcations that occur for the system without them. In the considered case, if we do not want to observe any bifurcations we should add damper with damping coefficient corresponding to 1.29% or more of critical damping or an inerter with 20 or more times bigger inertia than Duffing oscillator. Therefore, dampers are much more effective in canceling unwanted bifurcations. Moreover, addition of proper damper leads to increase of TMA's damping efficiency in a wide range of excitation frequencies while inerter can cause only slightly decrease of base structure amplitude. Simultaneously, combination of these two devices can lead to significant improvement of damping properties and enables much better control on the shape of FRCs. Therefore we can precisely adjust the response of considered structure to our expectations by selecting the right configuration of damper and inerter. In Section 4 we picked four different additional dampers and – for each – presented how the change of the inertance value influences response of Duffing oscillator. For every considered value of damping coefficient, decrease of the Duffing oscillator amplitude can be achieved by addition of a proper inerter. In the considered system, introduction of the inerter which has around half of Duffing oscillator inertia provides best damping properties despite the value of damping coefficient. Considering the fact that it is easier to obtain constant and precise value of inertance than damping coefficient, in many cases the combination of inerter and damper can be much more convenient to apply and enables better control of systems dynamics.

Acknowledgment

This work has been supported by Young Scientists Fund of Faculty of Mechanical Engineering at the Lodz University of Lodz.

Appendix A

In this section we consider the geometry of the system in detail as shown in Fig. 8.

To calculate forces generated by additional damper and inerter that are coupled to the arms of T-shaped pendulum we have to know the actual deformations of the devices. In order to derive formulas that describes how lengths of the devices change with the change in deflection of the pendulum we have to use geometrical measures of the system which are presented in Fig. 8. The angular displacements of pendulum are given by angle φ, the length of the arms of T-shaped pendulum is given by l_a, initial lengths of both devices are the same and described by parameter l_d. Actual length of expanding device will be described by l_1 and angle of its inclination by α_1. For contracting device we will use l_2, and α_2 respectively. Actual lengths of the devices are given by the following formulas:

$$l_1 = \frac{l_d}{\cos\alpha_1} + \frac{l_a \sin\varphi}{\cos\alpha_1} \tag{15}$$

$$l_2 = \frac{l_d}{\cos\alpha_2} - \frac{l_a \sin\varphi}{\cos\alpha_2} \tag{16}$$

Hence

$$l_1 \cos\alpha_1 = l_d + l_a \sin\varphi \tag{17}$$

$$l_2 \cos\alpha_2 = l_d - l_a \sin\varphi \tag{18}$$

Therefore we can get the following formulas:

$$\alpha_1 = \arccos\left(\frac{l_d + l_a \sin\varphi}{l_1}\right) \tag{19}$$

$$\alpha_2 = \arccos\left(\frac{l_d - l_a \sin\varphi}{l_2}\right) \tag{20}$$

To describe how design of the system influences the maximum values of angles α_1 and α_2 we introduce the following ratio:

$$l_{ratio} = \frac{l_d}{l_a} \tag{21}$$

Next we can determine actual lengths of the devices with the following formulas:

$$l_1 = l_a\sqrt{2 + l_{ratio}^2 - 2\cos\varphi + 2l_{ratio}\sin\varphi} \tag{22}$$

$$l_2 = l_a\sqrt{2 + l_{ratio}^2 - 2\cos\varphi - 2l_{ratio}\sin\varphi} \tag{23}$$

Substituting formulas (22), (23) (into 19) and (20) we obtain

$$\alpha_1 = \arccos\left(\frac{l_{ratio} + \sin\varphi}{\sqrt{2 + l_{ratio}^2 - 2\cos\varphi + 2l_{ratio}\sin\varphi}}\right) \tag{24}$$

$$\alpha_2 = \arccos\left(\frac{l_{ratio} - \sin\varphi}{\sqrt{2 + l_{ratio}^2 - 2\cos\varphi - 2l_{ratio}\sin\varphi}}\right) \tag{25}$$

In this paper we assume that in the described system, the angular displacement of pendulum is never greater than $\pi/2$ ($\varphi \le \pi/2$). Therefore in our case the maximum values of angles α_1 and α_2 can be observed for $\varphi = \pi/2$. In Fig. 9(a) we present how

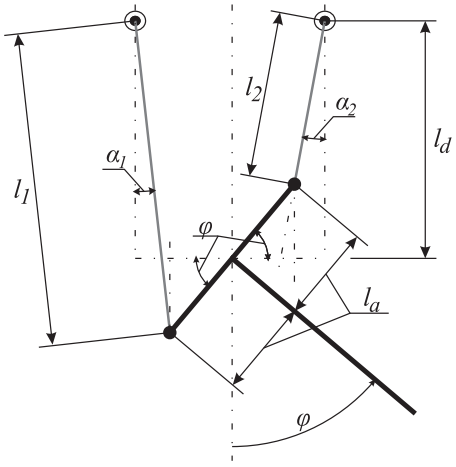

Fig. 8. Geometric measures that are used to describe actual lengths of devices.

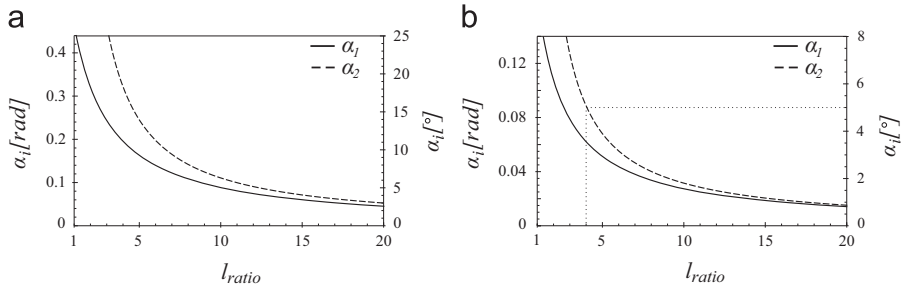

Fig. 9. Changes of angles $\alpha_1$and α_2 for $\varphi=\pi/2$ (a), and for $\varphi=\pi/4$ (a). Solid lines correspond to α_1, and dashed lines to α_2.

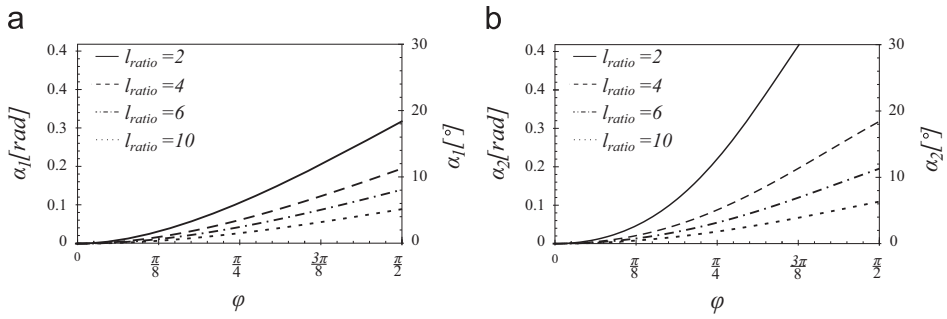

Fig. 10. Graphs showing how angles α_1 (a) and α_2 (b) changes with the change of angular displacement of the pendulum φ for different values of l_{ratio} parameter.

maximum values of angles α_1 and α_2 changes with the change of l_{ratio} when $\varphi=\pi/2$.

During optimization procedures we change value of inertance and damping coefficient of additional damper. Both of these devices cause a decrease in the amplitude of pendulum's motion. For chosen amplitude of excitation if damping coefficient is larger than 2% of critical damping, we do not observe angular deflections of pendulum greater than $\pi/4$ ($\varphi<\pi/4$). Hence in Fig. 9(b) we present how l_{ratio} influences the maximum values of angles α_1 and α_2 when $\varphi=\pi/4$. One can see that for $l_{ratio}>4$ both α_1 and α_2 are always smaller than 5°.

Analyzing formulas (24) and (25), one can see that values of angles α_1 and α_2 depend on two values: l_{ratio} which is constant and determined by the design of the system and angular displacement of the pendulum given by coordinate φ. In Fig. 10 we show how angle of pendulum's inclination influences angles α_1 and α_2 for four different values of l_{ratio} ($l_{ratio}=2$, $l_{ratio}=4$, $l_{ratio}=6$, $l_{ratio}=10$).

In our analysis we assume that $l_{ratio}=6$, therefore α_1 and α_2 can be treated as small angles. Due to this assumption we can introduce the following simplifications:

$$\begin{aligned} &\alpha_i \ll 1 \\ &\sin\alpha_i \simeq \alpha_i \qquad \cos\alpha_i \simeq 1 \qquad \text{for } i=1,2 \\ &\sin(\varphi\pm\alpha_i) \simeq \sin\varphi \qquad \cos(\varphi\pm\alpha_i) \simeq \cos\varphi \end{aligned} \tag{26}$$

References

[1] H. Frahm, Device for damping vibrations of bodies, US Patent US 989958 A, 1909.
[2] J.P. Den Hartog, Mechanical Vibrations, McGraw-Hill, New York, 1934.
[3] R.E. Roberson, Synthesis of a nonlinear dynamic vibration absorber, J. Frankl. Inst. 254 (1952) 205–220.
[4] F.R. Arnold, Steady-state behavior of systems provided with nonlinear dynamic vibration absorbers, J. Appl. Math. 22 (1955) 487–492.
[5] A.F. Vakakis, O.V. Gendelman, L.A. Bergman, D.M. McFarland, G. Kerschen, Y.S. Lee, Nonlinear Targeted Energy Transfer in Mechanical and Structural Systems, Solid Mechanics and Its Applications, vol. 156, Springer, Netherlands, 2009.
[6] Y. Starosvetsky, O.V. Gendelman, Vibration absorption in systems with a nonlinear energy sink: nonlinear damping, J. Sound Vib. 324 (2009) 916–939.
[7] E. Gourdon, N.A. Alexander, C.A. Taylor, C.H. Lamarque, S. Pernot, Nonlinear energy pumping under transient forcing with strongly nonlinear coupling: theoretical and experimental results, J. Sound Vib. 300 (2007) 522–551.
[8] H.R. Owji, A. Hossain Nezhad Shirazi, H. Hooshmand Sarvestani, A comparison between a new semi-active tuned mass damper and an active tuned mass damper, Proced. Eng. 14 (0) (2011) 2779–2787.
[9] M.M. Ali, K. Sun Moon, Structural developments in tall buildings: Current trends and future prospects, Arch. Sci. Rev. 50 (3) (2007) 205–223.
[10] S.-D. Kwon, K.-S. Park, Suppression of bridge flutter using tuned mass dampers based on robust performance design, J. Wind Eng. Ind. Aerodyn. 92 (2004) 919–934.
[11] M. Kitagawa, Technology of the akashi kaikyo bridge, Struct. Control Health Monit. 11 (2) (2004) 75–90.
[12] Y. Yang, J. Munoa, Y. Altintas, Optimization of multiple tuned mass dampers to suppress machine tool chatter, Int. J. Mach. Tools Manuf. 50 (9) (2010) 834–842.
[13] A. Rashid, C.M. Nicolescu, Design and implementation of tuned viscoelastic dampers for vibration control in milling, Int. J. Mach. Tools Manuf. 48 (9) (2008) 1036–1053.
[14] A. Ebrahimpour, R.L. Sack, A review of vibration serviceability criteria for floor structures, Comput. Struct. 83 (2005) 2488–2494.
[15] M. Setareh, R.D. Hanson, Tuned mass dampers for balcony vibration control, J. Struct. Eng. 118 (3) (1992) 723–740.
[16] P.L. Walsh, J.S. Lamancusa, A variable stiffness vibration absorber for minimization of transient vibrations, J. Sound Vib. 158 (2) (1992) 195–211.
[17] A.S. Alsuwaiyan, S.W. Shaw, Performance and dynamics stability of general-path centrifugal pendulum vibration absorbers, J. Sound Vib. 252 (5) (2002) 791–815.
[18] Y. Ishida, Recent developement of the passive vibration control method, Mech. Syst. Signal Process. 29 (2012) 2–18.
[19] R. Viguié, G. Kerschen, J.C. Golinval, D.M. McFarland, L.A. Bergman, A.F. Vakakis, N. van de Wouw, Using passive nonlinear targeted energy transfer to stabilize drill-string systems, Mech. Syst. Signal Process. 23 (1) (2009) 148–169.
[20] H. Hatwal, A.K. Mallik, A. Ghosh, Non-linear vibrations of a harmonically excited autoparametric system, J. Sound Vib. 81 (2) (1982) 153–164.
[21] H. Hatwal, A.K. Mallik, A. Ghosh, Forced nonlinear oscillations of an autoparametric system—Part 2: chaotic responses, J. Appl. Mech. 50 (3) (1983) 663–668.
[22] H. Hatwal, A.K. Mallik, A. Ghosh, Forced nonlinear oscillations of an autoparametric system—part 2: chaotic responses, J. Appl. Mech. 50 (3) (1983) 663–668.
[23] K. Bajaj, S.I. Chang, J.M. Johnson, Amplitude modulated dynamics of a resonantly excited autoparametric two degree-of-freedom system, Nonlinear Dyn. 5 (1994) 433–457.
[24] B. Banerjee, A.K. Bajaj, P. Davies, Resonant dynamics of an autoparametric system: a study using higher-order averaging, Int. J. Non-linear Mech. 31 (1) (1996) 21–39.

[25] M. Cartmell, J. Lawson, Performance enhancement of an autoparametric vibration absorber by means of computer control, J. Sound Vib. 177 (2) (1994) 173–195.
[26] K. Kecik, J. Warminski, Dynamics of an autoparametric pendulum-like system with a nonlinear semiactive suspension, Math. Probl. Eng. (2011).
[27] J. Warminski, K. Kecik, Autoparametric vibration of a nonlinear system with pendulum, Math. Probl. Eng. 2006 (2006) 80705.
[28] J. Warminski, J.M. Balthazar, R.M.L.R.F. Brasil, Vibrations of a non-ideal parametrically and self-excited model, J. Sound Vib. 245 (2) (2001) 363–374.
[29] J. Warminski, K. Kecik, Instabilities in the main parametric resonance area of a mechanical system with a pendulum, J. Sound Vib. 322 (3) (2009) 612–628.
[30] T. Ikeda, Nonlinear responses of dual-pendulum dynamic absorbers, J. Comput. Non-linear Dyn. 6 (1) (2011) 011012.
[31] Y. Song, H. Sato, Y. Iwata, T. Komatsuzaki, The response of a dynamic vibration absorber system with a parametrically excited pendulum, J. Sound Vib. 259 (4) (2003) 747–759.
[32] P. Brzeski, P. Perlikowski, S. Yanchuk, T. Kapitaniak, The dynamics of the pendulum suspended on the forced duffing oscillator, J. Sound Vib. 331 (2012) 5347–5357.
[33] R. Viguié, G. Kerschen, Nonlinear vibration absorber coupled to a nonlinear primary system: a tuning methodology, J. Sound Vib. 326 (3) (2009) 780–793.
[34] O. Fischer, Wind-excited vibrations - solution by passive dynamic vibration absorbers of different types, J. Wind Eng. Ind. Aerodyn. 95 (9) (2007) 1028–1039.
[35] F. Schilder, N.A. Alexander, Exploring the performance of a nonlinear tuned mass damper, J. Sound Vib. 319 (2009) 445–462.
[36] T. Ikeda, Bifurcation phenomena caused by multiple nonlinear vibration absorbers, J. Comput. Non-linear Dyn. 5 (2010) 021012.
[37] P. Brzeski, P. Perlikowski, T. Kapitaniak, Numerical optimization of tuned mass absorbers attached to strongly nonlinear duffing oscillator, Commun. Nonlinear Sci. Numer. Simul. 19 (1) (2014) 298–310.
[38] M.C. Smith, Synthesis of mechanical networks: the inerter, IEEE Trans. Autom. Control 47 (10) (2002) 1648–1662.
[39] F.-C. Wang, M.C. Smith, Performance benefits in passive vehicle suspensions employing inerters, Proceed. IEEE Conf. Decis. Control 3 (2004) 2258–2263.
[40] M.Z.Q. Chen, C. Papageorgiou, F. Scheibe, F.-C. Wang, The missing mechanical circuit element, Circuits Syst. Mag. IEEE 9 (1) (2009) 10–26.
[41] F.-C. Wang, W.-J. Su, Inerter nonlinearities and the impact on suspension control, In: American Control Conference, 2008, pp. 3245–3250.
[42] I. Takewaki, S. Murakami, S. Yoshitomi, M. Tsuji, Fundamental mechanism of earthquake response reduction in building structures with inertial dampers, Struct. Control Health Monit. 19 (6) (2012) 590–608.
[43] M.Z.Q. Chen, Y. Hu, L. Huang, G. Chen, Influence of inerter on natural frequencies of vibration systems, J. Sound Vib. 333 (7) (2013) 1874–1887.
[44] E.J. Doedel, A.R. Champneys, T.F. Fairgrieve, Y.A. Kuznetsov, B. Sandstede, X. Wang, Auto 97: continuation and bifurcation software for ordinary differential equations, 1998.